

# The nature of supermolecular bonds: Investigating hydrocarbon linked beryllium solvated electron precursors

Cite as: J. Chem. Phys. **156**, 194302 (2022); <https://doi.org/10.1063/5.0089815>

Submitted: 28 February 2022 • Accepted: 26 April 2022 • Accepted Manuscript Online: 26 April 2022 •  
Published Online: 16 May 2022

 Benjamin A. Jackson and  Evangelos Miliordos

## COLLECTIONS

Paper published as part of the special topic on [Nature of the Chemical Bond](#)



View Online



Export Citation



CrossMark

## ARTICLES YOU MAY BE INTERESTED IN

[Understanding the chemical bonding of ground and excited states of HfO and HfB with correlated wavefunction theory and density functional approximations](#)

The Journal of Chemical Physics **156**, 184113 (2022); <https://doi.org/10.1063/5.0090128>

[Disrupting bonding in azoles through beryllium bonds: Unexpected coordination patterns and acidity enhancement](#)

The Journal of Chemical Physics **156**, 194303 (2022); <https://doi.org/10.1063/5.0089716>

[Electron binding energies and Dyson orbitals of  \$O\_nH\_{2n+1}^{+,0,-}\$  clusters: Double Rydberg anions, Rydberg radicals, and micro-solvated hydronium cations](#)

The Journal of Chemical Physics **154**, 234304 (2021); <https://doi.org/10.1063/5.0053297>

Lock-in Amplifiers  
up to 600 MHz



Zurich  
Instruments



# The nature of supermolecular bonds: Investigating hydrocarbon linked beryllium solvated electron precursors

Cite as: J. Chem. Phys. 156, 194302 (2022); doi: 10.1063/5.0089815

Submitted: 28 February 2022 • Accepted: 26 April 2022 •

Published Online: 16 May 2022



View Online



Export Citation



CrossMark

Benjamin A. Jackson  and Evangelos Miliordos<sup>a)</sup> 

## AFFILIATIONS

Department of Chemistry and Biochemistry, Auburn University, Auburn, Alabama 36849-5312, USA

**Note:** This paper is part of the JCP Special Topic on Nature of the Chemical Bond.

<sup>a)</sup> Author to whom correspondence should be addressed: [emiliord@auburn.edu](mailto:emiliord@auburn.edu)

## ABSTRACT

Beryllium ammonia complexes  $\text{Be}(\text{NH}_3)_4$  are known to bear two diffuse electrons in the periphery of a  $\text{Be}(\text{NH}_3)_4^{2+}$  skeleton. The replacement of one ammonia with a methyl group forms  $\text{CH}_3\text{Be}(\text{NH}_3)_3$  with one peripheral electron, which is shown to maintain the hydrogenic-type shell model observed for  $\text{Li}(\text{NH}_3)_4$ . Two  $\text{CH}_3\text{Be}(\text{NH}_3)_3$  monomers are together linked by aliphatic chains to form strongly bound beryllium ammonia complexes,  $(\text{NH}_3)_3\text{Be}(\text{CH}_2)_n\text{Be}(\text{NH}_3)_3$ ,  $n = 1-6$ , with one electron around each beryllium ammonia center. In the case of a linear carbon chain, this system can be seen as the analog of two hydrogen atoms approaching each other at specific distances (determined by  $n$ ). We show that the two electrons occupy diffuse  $s$ -type orbitals and can couple exactly as in  $\text{H}_2$  in either a triplet or singlet state. For long hydrocarbon chains, the singlet is an open-shell singlet nearly degenerate with the triplet spin state, which transforms to a closed-shell singlet for  $n = 1$  imitating the  $\sigma$ -covalent bond of  $\text{H}_2$ . The biradical character of the system is analyzed, and the singlet-triplet splitting is estimated as a function of  $n$  based on multi-reference calculations. Finally, we consider the case of bent hydrocarbon chains, which allows the closer proximity of the two diffuse electrons for larger chains and the formation of a direct covalent bond between the two diffuse electrons, which happens for two  $\text{Li}(\text{NH}_3)_4$  complexes converting the open-shell to closed-shell singlets. The energy cost for bending the hydrocarbon chain is nearly compensated by the formation of the weak covalent bond rendering bent and linear structures nearly isoenergetic.

Published under an exclusive license by AIP Publishing. <https://doi.org/10.1063/5.0089815>

## I. INTRODUCTION

Metal ammonia complexes demonstrate the unique property of hosting diffuse electrons in their ground electronic states. These electrons populate hydrogenic-type orbitals in a shell model, which mimics that of the jellium or nuclear shell models.<sup>1</sup> For example,  $\text{Li}(\text{NH}_3)_4$  holds one electron in the periphery of the  $\text{Li}(\text{NH}_3)_4^+$  skeleton in an  $s$ -type orbital.<sup>2</sup> Even more interestingly, two such entities can bind together resembling the formation of  $\text{H}_2$  from two H atoms.<sup>2</sup> Aggregates of  $\text{Li}(\text{NH}_3)_4$  complexes form grids of  $\text{Li}(\text{NH}_3)_4^+$  cores with free, interstitial electrons, producing a metallic material known as an expanded or liquid metal.<sup>3,4</sup> We have named these metal ammonia complexes solvated electron precursors (SEPs) due to their presence in metal ammonia solutions of intermediate concentrations.<sup>5</sup>

The first systematic work on the Aufbau principle for the diffuse electrons in SEPs was reported for  $\text{Be}(\text{NH}_3)_4^{0,\pm}$  four years ago.<sup>1</sup>

The lowest energy orbital is  $1s$ , followed by  $1p$ ,  $1d$ ,  $2s$ ,  $1f$ , and  $2p$ . The adopted nomenclature was chosen to match the jellium or nuclear shell models. The same energy order has been observed for many other metals (including transition metals) clearly for the first three orbitals, but the  $2s$ ,  $2p$ , and  $1f$  orbitals are usually close in energy and their order may depend on the system.<sup>1,2,6-10</sup> In addition, two SEP molecules can bind together to form  $\sigma$  and  $\pi$  bonds similarly to traditional diatomic molecules.<sup>2</sup>

We recently showed that the replacement of one ammonia molecule with a methyl group enables the formation of SEPs for atoms where ammonia ligands alone are insufficient. Specifically, we demonstrated that  $\text{B}(\text{NH}_3)_4$  is unstable and ammonia cannot displace all three valence electrons of boron to the periphery of the complex.<sup>11</sup> Instead, one methyl group can form a B-C bond and three ammonia ligands can displace the remaining two electrons, to form a stable SEP. Furthermore, we proved that bridging two  $(\text{NH}_3)_3\text{BCH}_3$  entities by hydrocarbon chains forms stable

$(\text{NH}_3)_3\text{B}(\text{CH}_2)_n\text{B}(\text{NH}_3)_3$  linked-SEPs, hosting two diffuse electrons around each boron center. Currently, we examine the possibility to produce similar complexes with Be. Each beryllium center is expected to hold one diffuse electron, which leads to the questions: Do the two electrons couple into a triplet or singlet spin multiplicity? Do hydrocarbon chains bend to facilitate a chemical bond between the two electrons? What kind of orbitals are populated in the ground and excited electronic states? This work aims to answer these questions by means of density functional theory and multi-reference wavefunction methodologies. Exploration of this system will provide insight into the nature and stability of chemical bonding in supermolecular systems.

## II. COMPUTATIONAL DETAILS

All structures were optimized using density functional theory (DFT) and the CAM-B3LYP functional.<sup>12</sup> Correlation consistent triple- $\zeta$  basis sets were used for all atoms (cc-pVTZ). For hydrogen, an additional set of diffuse functions were used (aug-cc-pVTZ).<sup>13–15</sup> This methodology has been shown to provide excellent agreement with second-order Møller–Plesset perturbation theory (MP2) and coupled-clusters single, double, and perturbative triples, CCSD(T), structures for similar systems.<sup>10,16</sup> All reported species have only real frequencies. Single-point energy calculations at the MP2 level were used to further improve binding energies. The lowest energy singlet spin states were used for the geometry optimizations (unrestricted DFT = UDFT).

Excitation energies were calculated using state-averaged complete active space self-consistent field (SA-CASSCF) or simply CASSCF followed by second-order perturbation theory (CASPT2) as implemented in RS2C in MOLPRO 2015.1.<sup>17</sup> A level shift value of 0.2 a.u. and an IPEA (shift parameter for orbital energies) value of 0.25 a.u. were applied.<sup>18,19</sup> The basis sets used for the CASSCF/CASPT2 calculations of  $(\text{NH}_3)_3\text{Be}(\text{CH}_3)_n\text{Be}(\text{NH}_3)_3$  were cc-pVDZ (C, N, Be) and d-aug-cc-pVDZ (H).<sup>13–15,20</sup> For the linear  $n = 1–6$  and curved  $n = 1–4$  structures,  $C_{2h}$ ,  $C_{2v}$ , or  $C_2$  symmetry was imposed by rotation of  $\text{NH}_3$  groups. Symmetrical structures differ from the optimal geometries by less than 1 kcal/mol. For the  $n = 5, 6$  “curved” structures, optimal  $C_1$  geometries were used; and to ensure tractability of calculations for these two systems, the basis sets of the carbon and hydrogen atoms in the aliphatic chain included only s/p and s type functions, respectively. This approximation was proven to be very accurate for the excitation energies of the “linear”  $(\text{NH}_3)_3\text{Be}(\text{CH}_2)_6\text{Be}(\text{NH}_3)_3$  molecule (see below).

The active space for the reference CASSCF calculations consists of 1 electron in 10 orbitals for  $\text{CH}_3\text{Be}(\text{NH}_3)_3$ , two electrons in eight orbitals for “linear”  $(\text{NH}_3)_3\text{Be}(\text{CH}_2)_{1–6}\text{Be}(\text{NH}_3)_3$  species, two electrons in seven orbitals for “curved”  $(\text{NH}_3)_3\text{Be}(\text{CH}_2)_{1–5}\text{Be}(\text{NH}_3)_3$  species, and two electrons in six orbitals for “curved”  $(\text{NH}_3)_3\text{Be}(\text{CH}_2)_6\text{Be}(\text{NH}_3)_3$ . All states reported presently are averaged together with equal weights (SA-CASSCF); see Tables S10–S21 of the [supplementary material](#). All valence electrons are correlated at CASPT2. For the ground states, we also performed state specific CASSCF/CASPT2 calculations with two electrons in eight orbitals.

The cc-pVDZ (C, N, Be) and d-aug-cc-pVDZ (H) basis sets used for the excitation energies of “linear” and “curved”  $(\text{NH}_3)_3\text{Be}(\text{CH}_2)_{1–6}\text{Be}(\text{NH}_3)_3$  species were benchmarked for the  $\text{CH}_3\text{Be}(\text{NH}_3)_3$  monomer against the corresponding triple- $\zeta$  basis set

combination. The two sets agree within 0.04 eV, and double- $\zeta$  is considered quite accurate.

The multi-reference configuration interaction (MRCI) calculations for  $\text{BeCH}_3$  were done with the cc-pVTZ basis set for all atoms and the full valence space as active space for the reference CASSCF wavefunction. All four doublet spin states stemming from the first two Be +  $\text{CH}_3$  channels are averaged at the CASSCF level.

## III. RESULTS AND DISCUSSION

The ground state of Be ( $^1S$ ;  $1s^22s^2$ ) is of closed-shell nature but easily polarizable facilitating, for example, chemical bonds with other closed-shell systems such as  $\text{NH}_3$  or another Be atom.<sup>21</sup> An alternative path is the use of its first excited state  $^3P$  ( $1s^22s^12p^1$ ), which is  $21\,980\text{ cm}^{-1}$  higher ( $M_J$  averaged value from Ref. 22) than  $^1S$ . This is the case for the bond between Be and  $\text{CH}_3$ , which originates from Be ( $^3P$ ) +  $\text{CH}_3$  ( $\tilde{X}^2A'_2$ ). The potential energy curves (PECs) of the Be– $\text{CH}_3$  approach for all doublet states stemming from the first two adiabatic channels are shown in Fig. 1. The first excited state of  $\text{CH}_3$  is of the Rydberg character with the single electron populating the 3s orbital of carbon and lies at  $46\,239\text{ cm}^{-1}$ ; thus, the first two channels are Be ( $^1S$ ) +  $\text{CH}_3$  ( $\tilde{X}^2A'_2$ ) and Be ( $^3P$ ) +  $\text{CH}_3$  ( $\tilde{X}^2A'_2$ ). The quartet states from the second channel are either slightly attractive or repulsive at the CASSCF level and are not considered presently.

The ground state of  $\text{BeCH}_3$  is a doublet state with an unpaired electron in a primarily 2s orbital of beryllium polarized away from  $\text{CH}_3$ , avoiding the electron pair of the Be– $\text{CH}_3$  bond. The molecular orbitals of Fig. 2 illustrate the global minimum of  $\text{BeCH}_3$  that diabatically comes from Be( $^3P$ ) +  $\text{CH}_3$  ( $\tilde{X}^2A'_2$ ). The bonding scheme in Fig. 2 shows the bonding orbital between Be and  $\text{CH}_3$ .  $\text{CH}_3$  is initially planar<sup>23</sup> and as the two moieties approach each other, the unhybridized  $2p_z$  of carbon gradually mixes with the other valence orbitals to become an  $sp^3$  hybrid. The bonding orbital has a 0.61  $2p_z$

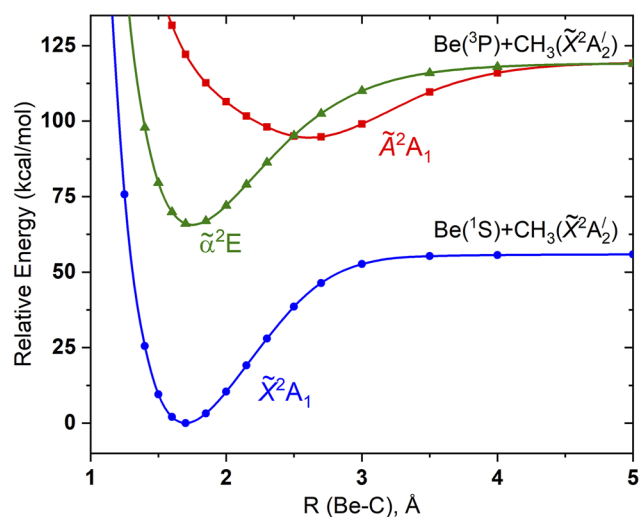
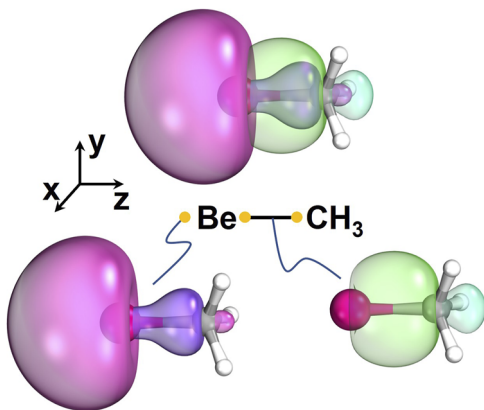


FIG. 1. MRCI potential energy curves for the Be– $\text{CH}_3$  approach as a function of the Be–C distance  $R(\text{Be}-\text{C})$ . All doublet spin states from the first two channels are shown, and the geometry of  $\text{CH}_3$  is kept fixed at the equilibrium  $\text{BeCH}_3$  geometry.



**FIG. 2.** Contours for the Be–C bonding and singly occupied molecular orbitals of the ground state of  $\text{BeCH}_3$ .

(C)  $-0.38$  2s (C)  $-0.60$  2s (Be)  $-0.45$  2p<sub>z</sub> (Be) composition and the singly occupied orbital  $0.73$  2s (Be)  $-0.67$  2p<sub>z</sub> (Be). The morphology of the PECs (see Fig. 1) is also in agreement with the proposed scheme revealing an avoided crossing between  $\tilde{X}^2A_1$  and  $\tilde{A}^2A_1$  in the region between 2.5 and 3 Å.

The Be–CH<sub>3</sub> bond is strong with a binding energy of 57.8 kcal/mol at the MP2 level of theory. The binding energy of the ammonia ligands is approximately half that: the first ammonia attaches to beryllium with 21.5 kcal/mol, the second one with 25.3 kcal/mol, and the third one with 26.3 kcal/mol. After zero-point energy corrections (at the CAM-B3LYP level), these MP2 binding energies become 18.6, 22.9, and 22.5 kcal/mol. The corresponding binding energies for  $\text{CH}_3\text{B}(\text{NH}_3)_3$ , which has two outer electrons, are considerably smaller at 8.6, 18.0, and 6.3 kcal/mol showing the difficulty that ammonia molecules have when displacing more than one electron.<sup>11</sup>

After the addition of three ammonia ligands to the metal center, the polarized 2s orbital of Be converts to a diffuse orbital at the “back” of the ammonia ligands. This orbital resembles the 1s outer orbital of  $\text{Li}(\text{NH}_3)_4$  but is polarized away from CH<sub>3</sub> (see Fig. 3). The first excited state is degenerate and pertains to the 1p<sub>x</sub> and 1p<sub>y</sub> peripheral orbitals (the z-axis is along the Be–C axis). The 1p<sub>z</sub><sup>1</sup> state is higher in energy and is polarized away from CH<sub>3</sub>. Similarly, the reduced symmetry [compared to the isolectronic tetrahedral  $\text{Li}(\text{NH}_3)_4$  complex] splits the 1d orbitals into three groups. The 1d<sub>xy</sub> and 1d<sub>x<sup>2</sup>-y<sup>2</sup></sub> remain degenerate and have the lowest energy among the 1d orbitals, degenerate 1d<sub>xz</sub> and 1d<sub>yz</sub> follow, and finally, 1d<sub>z<sup>2</sup></sub> is the highest energy 1d orbital. Lying among the 1d is the 2s orbital; clearly polarized toward the end of ammonia, it has an additional radial node with respect to 1s. These orbitals and relative energetics are depicted in Fig. 3.

The vertical excitation energies at the CASSCF and CASPT2 levels combined with triple- $\zeta$  quality basis sets for the mentioned states are listed in Table I. We also report SA-CASSCF orbital energies, and for CASPT2, we provide excitation energies with double- $\zeta$  quality basis sets. More detailed information is given in Tables S1 and S2 of the supplementary material. First, we comment on different datasets of excitation energies.  $\Delta E_{\text{orb}}$  are the excitation energies

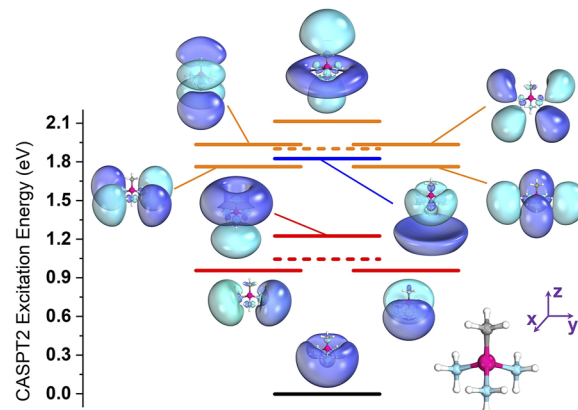


**FIG. 3.** Energy diagram (CASPT2 level of theory) and populated orbitals for the lowest energy electronic states of  $\text{CH}_3\text{Be}(\text{NH}_3)_3$ . The black line corresponds to the 1s orbital, the three solid red lines to the 1p orbitals, the blue line to the 2s orbital, and the five orange solid lines to the 1d orbitals. The red and orange dashed lines pertain to the average energies of 1p and 1d orbitals.

calculated as differences between the orbital energies at the CASSCF level. In the case of a strictly one-electron system, such as hydrogen, these will be identical to the CASSCF energies ( $\Delta E_{\text{CASSCF}}$ ).

A first observation is that the orbital energies apart from the 1s are all positive. Table I reveals that  $\Delta E_{\text{orb}}$  falls short of  $\Delta E_{\text{CASSCF}}$  by 0.14 eV for the first excited state  $\tilde{A}^2E$  and the discrepancy increases to 0.54 eV for  $\tilde{F}^2A_1$ . Therefore, the contribution/correlation with the  $\text{CH}_3\text{Be}(\text{NH}_3)_3^+$  electrons is substantial. CASPT2 increases further the vertical excitation energies by  $0.24 \pm 0.07$  eV depending on the electronic state (here and all following  $\pm$  is used to denote ranges in value). These demonstrate the need for high-level methods to accurately describe excitation energetics and CASPT2 has been shown to be equivalent to electron propagator and EOM (equation of motion)-CCSD levels of theory.<sup>1,24</sup> The difference in CASPT2 excitation energies between the double- $\zeta$  and triple- $\zeta$  basis sets is  $0.02 \pm 0.01$  eV, with the double- $\zeta$  values always smaller. This small difference justifies the use of double- $\zeta$  basis sets for the larger systems examined in later in this section.

**TABLE I.** Electronic states, electronic configurations, CASSCF orbital energies  $E_{\text{orb}}$  (eV), relative orbital energies  $\Delta E_{\text{orb}}$ , and vertical excitation energies (eV) at CASSCF ( $\Delta E_{\text{CASSCF}}$ ) and CASPT2 ( $\Delta E_{\text{CASPT2}}$ ) for  $\text{CH}_3\text{Be}(\text{NH}_3)_3$ .

State <sup>a</sup>	Config.	$E_{\text{orb}}$ <sup>b</sup>	$\Delta E_{\text{orb}}$ <sup>b</sup>	$\Delta E_{\text{CASSCF}}$ <sup>b</sup>	$\Delta E_{\text{CASPT2}}$ <sup>b</sup>	$\Delta E_{\text{CASPT2}}$ <sup>c</sup>
$\tilde{X}^2A_1$	1s <sup>1</sup>	-0.645	0.000	0.000	0.000	0.000
$\tilde{A}^2E$	1p <sup>1</sup>	0.003	0.648	0.792	0.959	0.942
$\tilde{B}^2A_1$	1p <sup>1</sup>	0.166	0.811	1.044	1.227	1.207
$\tilde{C}^2E$	1d <sup>1</sup>	0.495	1.140	1.489	1.765	1.731
$\tilde{D}^2A_1$	2s <sup>1</sup>	0.463	1.108	1.567	1.827	1.809
$\tilde{E}^2E$	1d <sup>1</sup>	0.566	1.211	1.633	1.937	1.900
$\tilde{F}^2A_1$	1d <sup>1</sup>	0.634	1.279	1.815	2.116	2.094

<sup>a</sup> Under  $C_{3v}$  point group.

<sup>b</sup> Basis set: cc-pVTZ(Be, N, C) d-aug-cc-pVTZ(H).

<sup>c</sup> Basis set: cc-pVDZ(Be, N, C) d-aug-cc-pVDZ(H).

Next, we compare the excitation energies of the isoelectronic “one-electron” systems  $\text{Li}(\text{NH}_3)_4$ ,  $\text{Be}(\text{NH}_3)_4^+$ , and  $\text{CH}_3\text{Be}(\text{NH}_3)_3$ . The first system has a  $\text{Li}^+$  center, and the second one has a  $\text{Be}^{2+}$  center. Therefore, excitation energies of  $\text{Be}(\text{NH}_3)_4^+$  are expected to be greater. Comparing the two, excitations from 1s to 1p, 1d, and 2s are 0.72, 1.42, and 1.52 eV for  $\text{Li}(\text{NH}_3)_4$  and 1.39, 2.37, and 3.34 eV for  $\text{Be}(\text{NH}_3)_4^+$ ,<sup>1,2</sup> confirming this expectation. The corresponding excitation energies for  $\text{CH}_3\text{Be}(\text{NH}_3)_3$  are 1.05 (averaged over all 1p states), 1.90 (averaged over all 1d states), and 1.81 eV. These values fall in between those for  $\text{Li}(\text{NH}_3)_4$  and  $\text{Be}(\text{NH}_3)_4^+$ , indicating an intermediate formal charge on Be.

The use of a methyl group in the first coordination sphere of Be enables the formation of stable beryllium ammonia monomers, which are bridged by hydrocarbon chains, to give the dimeric  $(\text{NH}_3)_3\text{Be}(\text{CH}_2)_n\text{Be}(\text{NH}_3)_3$ . Given that the  $\text{BeCH}_3(\text{NH}_3)_3$  complex behaves as an analog of a hydrogen atom, the hydrocarbon chain length permits the study of the chemical nature of supermolecular SEP bond formation comparable to the formation of  $\text{H}_2$  from the fixed approach of two radical H atoms. A range of hydrocarbon chain lengths (1–6 carbon atoms) was employed to examine the spin coupling of the two electrons as a function of their “distance,” one located about each  $\text{BeCH}_2(\text{NH}_3)_3$  moiety. These can couple into a triplet and open-shell or closed-shell singlet. Long chains are expected to favor the triplet state with the open-shell singlet state being slightly above or nearly degenerate to the triplet while shorter chains are expected to prefer the closed-shell singlet and form a covalent SEP bond. These expectations are based on the mechanism of  $\text{H}_2$  formation.

The carbon chain length can grow in two ways, either in a “linear” fashion keeping every C–C bond in a staggered conformation, or in a “curved” fashion that allows different conformations for

each C–C bond, which reduces the Be–Be distance and promotes the SEP–SEP interaction. We begin with the discussion of linear systems. Figure 4 depicts the optimal geometries for the “linear”  $(\text{NH}_3)_3\text{Be}(\text{CH}_2)_n\text{Be}(\text{NH}_3)_3$  species ( $n = 1–6$ ). The dimers with an odd number of carbons are  $C_{2v}$  while even are  $C_{2h}$  in structure. The binding energies of the ammonia molecules to beryllium are slightly affected by the presence of the chain or the second beryllium–ammonia complex. Specifically, we calculated the binding energy of each ammonia by sequentially adding ammonia ligands (see Tables S4–S9 of the supplementary material for geometries and Table S10 for energies). The binding energies for an ammonia ligand to bind to beryllium ranging between 19.5 and 27.2 kcal/mol for all cases except four values belonging to the smallest species ( $n = 1–2$ ; see Table S10 of the supplementary material). These are practically identical to the binding energies for  $\text{CH}_3\text{Be}(\text{NH}_3)_3$  (21.5–26.3 kcal/mol; see above). A similar observation was made for the boron analog.<sup>11</sup>

The orbitals populated in the lowest electronic states and their energy are shown in Fig. 5. The in- and out-of-phase combination of the two outer 1s orbitals produces the  $\sigma_s$  and  $\sigma_s^*$  orbitals. Similarly, the  $1p_x$  and  $1p_y$  orbitals (the z axis considered along the Be–Be line) generate the  $\pi_{x,y}$  and  $\pi_{x,y}^*$  orbitals. Finally, the  $1p_z$  orbitals make the  $\sigma_z$  and  $\sigma_z^*$  orbitals, which are the highest energy ones as they are highly deformed in the presence of the carbon chain. The lowest lying electronic states are investigated with CASPT2 and our complete list for all six species of Fig. 4 is given in Tables S10–S15 of the supplementary material. Table II summarizes our findings reporting excitation energies and electronic configurations.

The electronic configuration of the ground states consists of two major components  $\sigma_s^2$  and  $\sigma_s^{*2}$ , where  $\sigma_s \approx 1s_L + 1s_R$  and  $\sigma_s^* \approx 1s_L - 1s_R$ , with  $1s_L$  and  $1s_R$  being the outer 1s orbitals of the left and right terminus, respectively. The weight of the two components

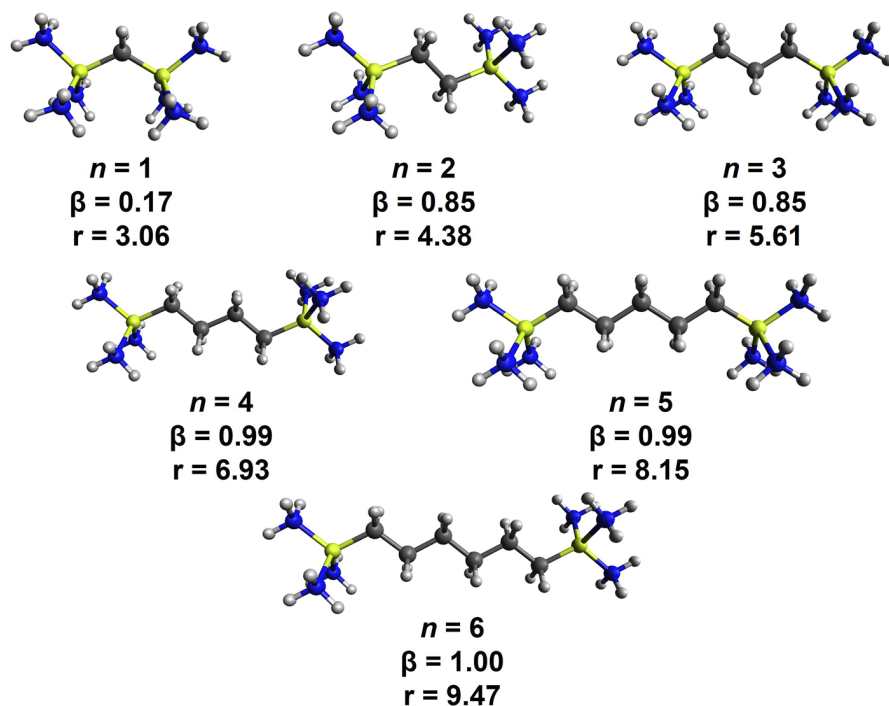


FIG. 4. Optimized geometries for the “linear”  $(\text{NH}_3)_3\text{Be}(\text{CH}_2)_n\text{Be}(\text{NH}_3)_3$  species with  $n = 1–6$ . The biradical character  $\beta$  and the Be–Be distance  $r$  (in Å) for each species are also reported.

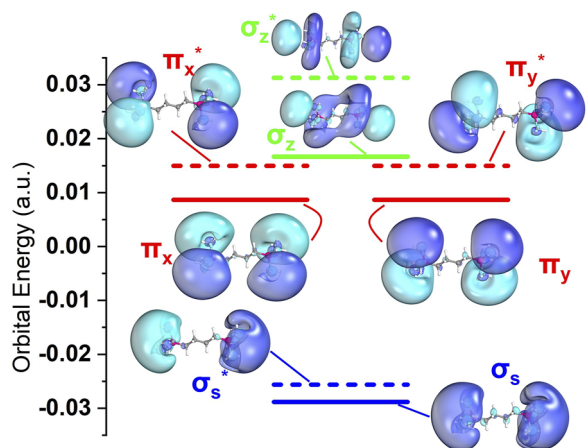


FIG. 5. Orbitals for the outer orbitals of the "linear"  $(\text{NH}_3)_3\text{Be}(\text{CH}_2)_n\text{Be}(\text{NH}_3)_3$  species.

changes with the number  $n$  of carbon atoms in the hydrocarbon chain. It can be proven that when these two coefficients are equal in magnitude but have opposite signs, then the electronic configuration can be equally described as  $1s_L^1 1s_R^1$  (open-shell singlet biradical) instead of  $\sigma_s^2 - \sigma_s^{*2}$ .<sup>25</sup> Of course when one of the two coefficients is zero, then we have a closed-shell system. For intermediate cases ( $c_1 \sigma_s^2 - c_2 \sigma_s^{*2}$ ), the biradical character  $\beta$  can be estimated as  $2c_2^2/(c_1^2 + c_2^2)$  with a value of 1.00 meaning 100% biradical.<sup>25</sup> It should be added that our UDFT calculations for the singlet states of the longer species converge to the broken symmetry solution  $1s_L^1 1s_R^1$  (open-shell singlet). The spin contamination is relatively

TABLE II. Electronic states, electronic configurations, and CASPT2 vertical excitation energies (eV) for "linear"  $(\text{NH}_3)_3\text{Be}(\text{CH}_2)_n\text{Be}(\text{NH}_3)_3$ .

State <sup>a</sup>	Config.	$n = 1$	$n = 2$	$n = 3$	$n = 4$	$n = 5$	$n = 6$
$^1A_1/^1A_g$ <sup>b</sup>	$\sigma_s^2/\sigma_s^{*2}$	0.00	0.00	0.00	0.00	0.00	0.00
$^3B_2/^3B_u$ <sup>c</sup>	$\sigma_s^1 \sigma_s^{*1}$	0.33	0.03	0.02	0.00	0.00	0.00
$^3B_1/^3B_u$ <sup>d</sup>	$\sigma_s^1 \pi^1/\sigma_s^{*1} \pi^{*1}$	0.57	0.76	0.78	0.90	0.89	0.93
$^3A_1/^3A_u$ <sup>e</sup>	$\sigma_s^1 \pi^1/\sigma_s^{*1} \pi^{*1}$	0.70	0.70	0.76	0.87	0.89	0.91
$^1B_2/^1B_g$ <sup>f</sup>	$\sigma_s^{*1} \pi^1/\sigma_s^1 \pi^{*1}$		0.81	0.75	0.88	0.89	0.91
$^1A_2/^1A_g$ <sup>f</sup>	$\sigma_s^{*1} \pi^1/\sigma_s^1 \pi^{*1}$		0.85	0.86	0.90	0.89	0.93

<sup>a</sup>Under  $C_{2v}/C_{2h}$  point groups for odd/even  $n$  values.

<sup>b</sup>The CI coefficients for the  $\sigma_s^2/\sigma_s^{*2}$  configurations are 0.89/−0.28, 0.75/−0.60, 0.73/−0.60, 0.69/−0.68, 0.68/−0.68, and 0.69/−0.68 for  $n = 1$ –6.

<sup>c</sup>The CI coefficients are 0.96–0.97 for all  $n$  values. More accurate excitation energies are 3052.4, 116.0, 58.3, −0.3, and  $0.5 \text{ cm}^{-1}$  (state specific CASSCF/CASPT2; see Table S30 of supplementary material).

<sup>d</sup>The CI coefficients for  $\sigma_s^1 \pi^1$  range from 0.70 ( $n = 6$ ) to 0.97 ( $n = 1$ ). For  $n \geq 2$ , there is significant contribution from a  $\sigma_s^{*1} \pi^{*1}$ ; CI coefficients range from −0.47 ( $n = 2$ ) and −0.69 ( $n = 6$ ).

<sup>e</sup>The CI coefficients for  $\sigma_s^1 \pi^1$  range from 0.71 ( $n = 6$ ) to 0.97 ( $n = 1$ ). For  $n \geq 2$ , there is significant contribution from a  $\sigma_s^{*1} \pi^{*1}$ ; CI coefficients range from −0.39 ( $n = 2$ ) and −0.69 ( $n = 6$ ).

<sup>f</sup>These states are highly multi-reference, and both configurations have CI coefficients of the 0.44–0.54 range.

large ( $\langle S^2 \rangle = 1$ ), but the optimized geometry is not affected and is identical to the degenerate triplet state. Therefore, we consider that our UDFT calculated geometries are a good compromise avoiding computationally demanding CASPT2 geometry optimizations.

We expect that the longer the chain is, the larger the  $\beta$  values are, since the two terminal electrons become more and more "independent" (smaller overlap between the two outer  $1s$  orbitals). The obtained  $\beta$  values are given and plotted in Fig. 6 and generally follow the expected trend. For  $n = 1$ , our value is 0.17 indicating a predominately closed-shell system, but for  $n = 2$  and 3, we obtain two identical values 0.85 and 0.85. We believe that this is due to the fact that the  $C_{2v}$  geometry of odd  $n$  values brings four out of the six ammonia ligands to the same side facilitating a larger overlap between the two outer  $1s$  orbitals (see inset of Fig. 6) and, thus, decreasing the biradical character. Therefore, the species with  $n = 3$  has a smaller biradical character than expected. Within the odd and even  $n$  values, the  $\beta$  values increase smoothly to one.

The first excited state has a  $\sigma_s^1 \sigma_s^{*1}$  triplet spin character, which can also be described as a  $1s_L^1 1s_R^1$  triplet state. The singlet-triplet energy splitting ( $\Delta E_{1et-3et}$ ) for the  $n = 1$ –6 series drops as  $\beta$  and  $n$  increase as has been seen for similar systems (OXO, X =  $\text{CH}_2$ , NH, O,  $\text{F}^+$ ).<sup>25</sup> The  $\Delta E_{1et-3et}$  values are 3052.4, 116.0, 58.3, −0.3, 0.5, and  $0.03 \text{ cm}^{-1}$  for  $n = 1$ –6 (state specific CASSCF + CASPT2; see Table S30 of the supplementary material). Using the  $n = 1, 3$  species, the slope of  $\Delta E_{1et-3et}$  vs  $\beta$  is  $430.2 \text{ cm}^{-1}$  per 10% biradical character. Practically, for  $n \geq 4$ , we have a pure open-shell singlet state.

Table II lists the CASPT2 excitation energies and configurations of a few more electronic states (see Tables S10–S15 of the supplementary material for more states and absolute energies). The next two states ( $^3B_1$  and  $^3A_1$  for  $n = \text{odd}$ ;  $^3B_u$  and  $^3A_u$  for  $n = \text{even}$ ) are triplets of primarily  $\sigma_s^1 \pi^1$  character. For  $n = 1$ , these are pure  $\sigma_s^1 \pi^1$  states but as  $n$  increases contributions of  $\sigma_s^{*1} \pi^{*1}$  configurations

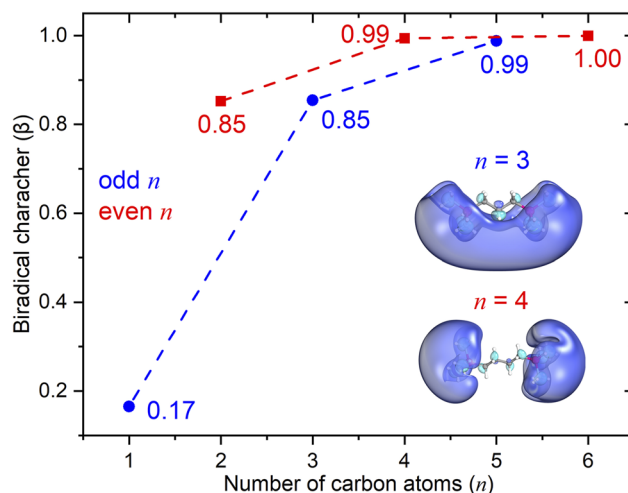


FIG. 6. Biradical character as a function of  $n$  for the "linear"  $(\text{NH}_3)_3\text{Be}(\text{CH}_2)_n\text{Be}(\text{NH}_3)_3$  species with  $n = 1$ –6. The  $\sigma_s$  orbitals for  $n = 3$  and 4 are depicted as insets.

also increase. This is explained as  $\sigma_s$  trends to degeneracy with  $\sigma_s^*$  for increasing  $n$ ; the same occurs for  $\pi$  and  $\pi^*$  and  $\sigma_z$  and  $\sigma_z^*$  (see Fig. 4 of Ref. 11). Because of this, all states become increasingly multi-reference as  $n$  increases. These two triplets lie at 0.57 and 0.70 eV for  $n = 1$ , are nearly degenerate for  $n = 2, 3$  at  $\sim 0.75$  eV, and, finally, become degenerate for  $n \geq 4$  at  $\sim 0.90$  eV. The next two states ( $^1B_2$  and  $^1A_2$  for  $n = \text{odd}$ ;  $^1B_g$  and  $^1A_g$  for  $n = \text{even}$ ) are mixtures of different  $\sigma_s^* \pi^1 / \sigma_s^* \pi^* \pi^1$  components, which contribute to coefficients in the 0.44–0.54 range. These are practically degenerate for all species at 0.8–0.9 eV. The remaining states are multi-configurational and involve excitations to  $\sigma_z$  and  $\sigma_z^*$  as well (see Tables S10–S15 of the [supplementary material](#)).

The two terminal electrons in the ground state can, in principle, induce the bending of the hydrocarbon chains, bringing the two Be centers closer to form a covalent bond as happens for two  $\text{Li}(\text{NH}_3)_4$  complexes.<sup>2</sup> Similar binding has been reported for methylated ammonium derivatives, connected with hydrocarbon chains.<sup>26,27</sup> Thus, we performed geometry optimizations for “curved”  $(\text{NH}_3)_3\text{Be}(\text{CH}_2)_{2-6}\text{Be}(\text{NH}_3)_3$  structures and found that such species are possible and energetically competitive compared to the “linear” isomers. For example, the rotation around the C–C bond of the  $(\text{NH}_3)_3\text{Be}(\text{CH}_2)_2\text{Be}(\text{NH}_3)_3$  species brings the two beryllium ammonia units to a Gauche position (compare Figs. 4 and 7). The energy of the “curved” (Gauche) structure is 1.6 kcal/mol lower at MP2, and the biradical character decreases from 0.85 to 0.22 (see Table S17 for CI coefficients).

Similar trends are found for the larger “curved” species shown in Fig. 7. The relative stability of “linear” and “curved” species depends mainly on two factors: The strain energy that accumulates when a C–C bond rotates from the trans to the Gauche position and the binding energy for the two unpaired electrons. The latter is larger when the two beryllium-ammonia terminals are closer and the three ammonia ligands of each unit point to the three ammonia ligands of the other unit.<sup>2</sup> This arrangement seems to maximize the solvation energy of the formed electron pair in the middle of the two beryllium ammonia units (see Refs. 2 and 5). For instance, the binding energy for two  $\text{Li}(\text{NH}_3)_4$  complexes in the optimal arrangement is 10–15 kcal/mol<sup>2</sup>, and the trans-Gauche strain energy for each C–C bond is 0.6 kcal/mol.<sup>28</sup>

The structures of Fig. 7 are the lowest energy “curved” species that we were able to locate but a more systematic work may be necessary for definitive conclusions. In addition to the optimal structures, Fig. 7 reports also the energy difference at CASPT2  $\Delta E$  from the “linear” isomers, the biradical character  $\beta$ , and the Be–Be distance  $r$  (see Table S30 of the [supplementary material](#)). None of the  $\text{Be}(\text{NH}_3)_3 \cdots (\text{NH}_3)_3\text{Be}$  interactions adopts the optimal arrangement found for two  $\text{Li}(\text{NH}_3)_4$  complexes mainly due to the short hydrocarbon chain, which does not allow the better solvation of the formed electron pair. In addition, the  $\Delta E$  values are always positive indicating that the “curved” species are lower in energy. Therefore, the SEP-SEP attraction is expected to be of the order of a few kcal/mol and higher than the developed strain energy of the hydrocarbon chain.

The biradical character is considerably lower for the “curved” isomers indicating partial bonding between the two unpaired electrons. For  $n = 2$  goes from 0.85 to 0.22, for  $n = 3$  from 0.85 to 0.64, for  $n = 4$  from 0.99 to 0.63, for  $n = 5$  from 0.99 to 0.39, and for  $n = 6$  from 1.00 to 0.25. The most impressive difference is that for

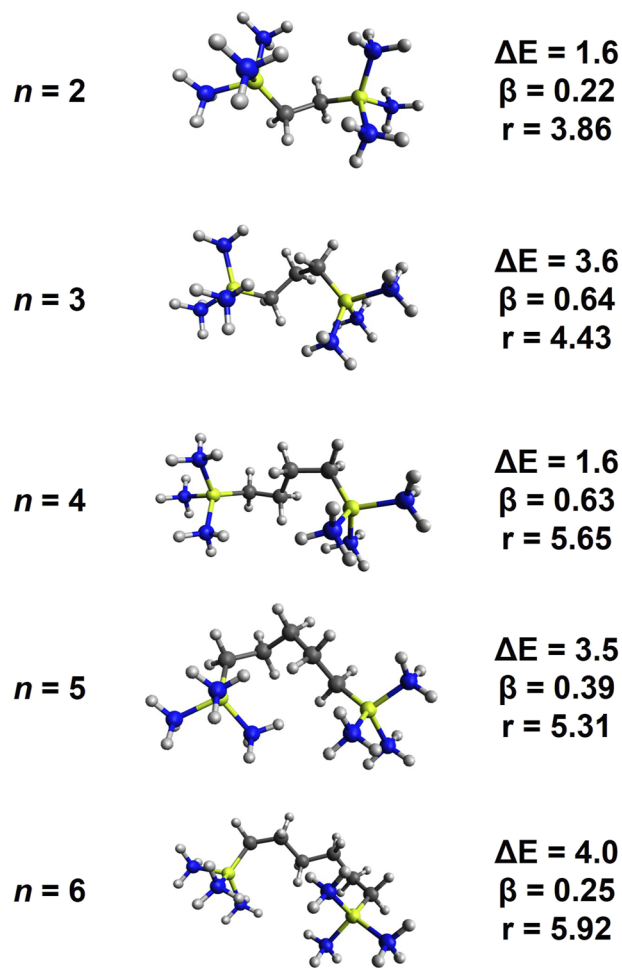


**FIG. 7.** CAM-B3LYP geometries for the “curved”  $(\text{NH}_3)_3\text{Be}(\text{CH}_2)_n\text{Be}(\text{NH}_3)_3$  species for  $n = 2$ –6. The energy difference from the lower energy “linear” isomers  $\Delta E$  (in kcal/mol; “curved” structures are always more stable than “linear”) at CASPT2 (see Table S30 of the [supplementary material](#)), the biradical character  $\beta$ , and the Be–Be distance  $r$  (in Å) for each species are also reported.

$n = 5, 6$ , where the two single electrons of the “curved” isomer form almost exclusively a two-electron bond. The structure of “curved”  $(\text{NH}_3)_3\text{Be}(\text{CH}_2)_6\text{Be}(\text{NH}_3)_3$  (see Fig. 7) has four ammonia ligands and four N–H bonds solvating the electron pair localized in the middle of the molecule (see Fig. S1 of the [supplementary material](#)). Furthermore, the  $r$  value of 5.92 Å for  $n = 6$  is nearly identical to the Li–Li distance of  $\sim 6$  Å found for  $[\text{Li}(\text{NH}_3)_4]_2$ . The species with  $n = 3, 4$  have a smaller number of directional N–H bonds solvating the electron pair and, thus, a larger radical character ( $\beta = 0.63$ –0.64).

For “curved” systems, we also provide excitation energies for the lowest energy states listed in Tables S16–S20 of the [supplementary material](#). These states involve  $\sigma_s$ ,  $\sigma_s^*$ ,  $\pi$ , and  $\pi^*$  orbitals like those in Fig. 5. Notably, the “curved” species generally have a larger number of excited states within 1.0 eV compared to the “linear.” For example, the “linear”  $n = 6$  species has two quasi-degenerate ground states followed by the lowest energy states at 0.91–0.97 eV

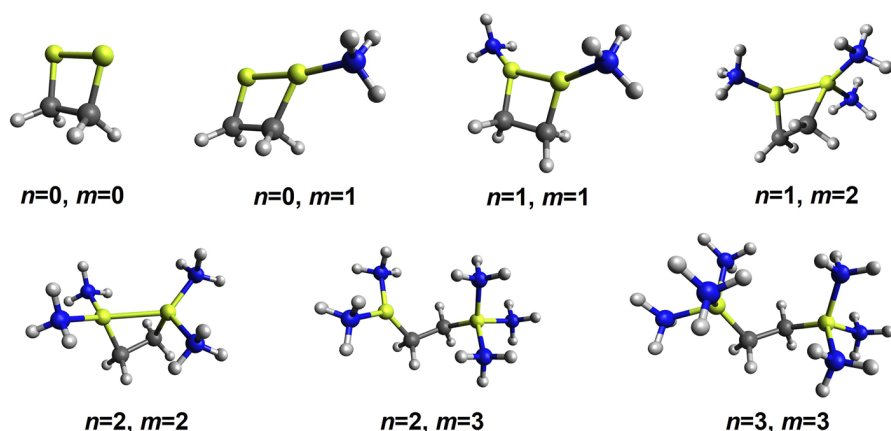


FIG. 8. CAM-B3LYP geometries for the sequential addition of ammonia ligands to  $(\text{CH}_2)_2\text{Be}_2$  to form  $(\text{NH}_3)_n\text{Be}(\text{CH}_2)_2\text{Be}(\text{NH}_3)_m$  and finally  $(\text{NH}_3)_3\text{Be}(\text{CH}_2)_2\text{Be}(\text{NH}_3)_3$ .

(see Table II and Tables S10–S15 of the [supplementary material](#)), but the “curved” isomer has five states with excitation energies spread almost evenly within 1.0 eV (0.22, 0.58, 0.74, 0.85, and 1.02 eV; see Table S21 of the [supplementary material](#)). This pattern mimics the excitation energies pattern of  $[\text{Li}(\text{NH}_3)_4]_2$  (0.59, 0.66, 0.92, 1.13 eV). This trend can guide future experimental work in distinguishing and identifying the “curved” and “linear” species.

Due to the lack of symmetry in “curved”  $n = 5, 6$  structures and to enable CASTP2 calculations for these systems, we employed minimal cc-pVDZ basis sets for the C and H atoms of the hydrocarbon chain with only s function on H and s and p functions on C. The basis sets for other atoms remained the same. To validate this choice, we compare excitation energies for “linear”  $n = 6$  species using the full cc-pVDZ(Be,N,C) d-aug-cc-pVTZ(H) basis set vs the same basis set with the minimal basis cc-pVDZ. The results listed in Table S22 of the [supplementary material](#) show that the excitation energies are affected by at most 0.01 eV justifying the use of the smaller basis set for the excitation energies of “curved”  $n = 5, 6$  species (Tables S19–S20 of the [supplementary material](#)).

Finally, we studied the formation process of the  $(\text{NH}_3)_3\text{Be}(\text{CH}_2)_{1-6}\text{Be}(\text{NH}_3)_3$  species starting from  $\text{Be}(\text{CH}_2)_{1-6}\text{Be}$  depleted of ammonia ligands. These unsaturated species for  $n = 2$  are depicted in Fig. 8. As expected, the two Be atoms bind to each other making a cyclic  $(\text{CH}_2)_2\text{Be}_2$  molecule. The addition of one ammonia ligand leads to stabilization by 41 kcal/mol (at MP2) and shortening of the Be–Be bond length from 1.97 to 1.92 Å. The second ammonia elongates the Be–Be bond to 2.09 Å, and the third one shortens it to 2.02 Å. The addition of more ammonia ligands finally induces the dissociation of the Be–Be bond increasing the Be–Be distance to 2.37 ( $n = 4$ ), 3.57 ( $n = 5$ ), and 3.79 ( $n = 6$ ) Å. The same trends are seen for larger aliphatic chains. All geometries for  $(\text{NH}_3)_n\text{Be}(\text{CH}_2)_{1-6}\text{Be}(\text{NH}_3)_m$  are given in Tables S22–S26 of the [supplementary material](#). The binding energy for the first ammonia ligand is always the largest, ranging from 25 to 41 kcal/mol. On average, the binding energy for the remaining ammonia is 15–16 kcal/mol. The cyclic structures are always lower in energy than the corresponding open ended “linear” species (no Be–Be bond occurs), and this difference increases with  $n$ . For  $n = 2–6$ , the  $\Delta E$  of the “linear” and “curved”  $\text{Be}(\text{CH}_2)_n\text{Be}$  is 15.0, 28.9, 40.9, 45.9,

and 51.8 kcal/mol. As ammonia ligands are added and the Be–Be bond length increases, the relative difference between “linear” and “curved” decreases until saturation when the difference is 1.6–4.0 kcal/mol.

Based on these results, we can show that the character of supermolecular bonds in this system is dependent on two things: the length of SEP separation and the orientation of ammonia groups. The results of the “linear” system depict a predominantly closed-shell configuration as the two electrons couple to form a covalent SEP–SEP bond for  $n = 1$  with a Be–Be distance of 3.1 Å and a biradical character  $\beta = 0.18$ . As  $n$  increases, the system becomes increasingly biradical in character. The Be–Be distance for  $n = 2, 3$  is 4.4 and 5.6 Å while  $\beta = 0.78$  and 0.81, respectively. At  $n = 4$ , the two Be atoms are separated by 6.9 Å and the two SEP electrons act as separate systems rather than bonding groups. For the “curved” systems, the covalent bonding character is much larger as the positioning of ammonia ligands improves solvation of the electron pair between the SEP centers. This is starkly seen for  $n = 6$  where four ammonia ligands and four N–H bonds solvating the electron pair drop  $\beta$  from 1.00 in the “linear” to 0.25 in the “curved.” In other words, converting the localized radical electrons to a nearly pure covalent bond. Within the “linear” systems, the effect of amine orientation is also seen in the case of  $n = 2$  and 3 where, despite the longer distance of  $n = 3$ , the two have nearly equivalent  $\beta$ , which is explained by the  $C_{2v}$  geometries having four out of the six ammonia ligands on the same side facilitating a larger overlap between the two outer 1s orbitals. Current results appear to indicate that the SEP–SEP binding energy is not able to offset the steric strain induced by the chain curving. As chain length increases further, it is expected that the curved structure will win out due to decreased steric strain.

#### IV. SUMMARY AND CONCLUSIONS

In this work, we examined the electronic structure for the ground and excited states of  $\text{CH}_3\text{Be}(\text{NH}_3)_3$ , which is isovalent to  $\text{Li}(\text{NH}_3)_4$  and  $\text{Be}(\text{NH}_3)_4^+$ . These species have one peripheral electron delocalized around the first coordination sphere of the metal. The methyl group captures one beryllium electron and facilitates the coordination of three ammonia ligands and the displacement of the

remaining beryllium electron to the periphery. This electron populates s-, p-, and d-type orbitals as in  $\text{Li}(\text{NH}_3)_4$ , but the p- and d-type orbitals are not degenerate or quasi-degenerate anymore; the orbitals along the Be–C axis are destabilized going to higher energies. Overall, the excitation energies of  $\text{CH}_3\text{Be}(\text{NH}_3)_3$  fall in-between those of  $\text{Li}(\text{NH}_3)_4$  and  $\text{Be}(\text{NH}_3)_4^+$ . The double- $\zeta$  quality basis sets are shown to give comparable excitation energies with triple- $\zeta$  and are applied for the larger systems of  $(\text{NH}_3)_3\text{Be}(\text{CH}_2)_n\text{Be}(\text{NH}_3)_3$ . We show that two  $\text{CH}_3\text{Be}(\text{NH}_3)_3$  monomers can be linked together by aliphatic chains to form strongly bound beryllium ammonia complexes,  $(\text{NH}_3)_3\text{Be}(\text{CH}_2)_n\text{Be}(\text{NH}_3)_3$ ,  $n = 1-6$ , with one electron around each beryllium ammonia center, the analysis of which is used to provide insight into the chemical bonding of supermolecular systems such as SEPs. The hydrocarbon chain is shown to exist either in a “linear” structure in a “curved” structure to promote interaction between the SEP centers. In the linear system, the spin coupling into a closed-shell singlet is strong for  $n = 1$ , partial for  $n = 2, 3$ , and non-existent for  $n \geq 4$ , where the two electrons couple clearly to an open-shell singlet. This trend reflects the biradical character  $\beta$  and the singlet-triplet splitting. The singlet-triplet splitting is relatively large for  $n = 1$ , small for  $n = 2, 3$ , and practically zero for  $n \geq 4$ . Higher energy electronic states populate  $\pi$ -,  $\pi^*$ -,  $\sigma_z$ -, and  $\sigma_z^*$ -type orbitals resembling those of traditional diatomic systems, and they are highly multi-reference states. In the curved system, the coupling is strong for the more flexible  $n = 6$  case and for the  $n = 2$  case, where the two electrons are in close proximity. However, the curved structures are found to be lower in energy by a few kcal/mol. We also found that the quality of the basis set of the H and C atoms of the hydrocarbon chain is small in the excitation energies and allows for the use of minimal basis sets for these atoms. In addition, we studied the formation mechanism of the dimeric species starting from the cyclic  $\text{Be}_2(\text{CH}_2)_{1-6}$  molecules and adding ammonia ligands sequentially. Initially, a cyclic structure is favored with a Be–Be bond and the ammonia ligands bind rigorously to beryllium with each resulting in a weakening of the Be–Be bond until it is fully broken at ligand saturation. We believe that our calculations can reveal the existence of novel materials composed of metal centers with diffuse electrons. Such materials can be used as redox catalysts or for quantum computing purposes.

## SUPPLEMENTARY MATERIAL

See the [supplementary material](#) for geometric structures, electronic configurations, excitation energies, and orbitals for the ground and several excited states of the linear and curved species.

## ACKNOWLEDGMENTS

The authors are indebted to Auburn University (AU) for financial support. E.M. is especially grateful to the donors of the James E. Land endowment. This work was completed with resources provided by the Auburn University Hopper and Easley Clusters. This work was supported by the National Science Foundation under Grant No. CHE-1940456.

## AUTHOR DECLARATIONS

### Conflict of Interest

The authors have no conflicts to disclose.

## DATA AVAILABILITY

The data that support the findings of this study are available within the article and its [supplementary material](#).

## REFERENCES

- 1 I. R. Ariyaratna, S. N. Khan, F. Pawłowski, J. V. Ortiz, and E. Miliordos, *J. Phys. Chem. Lett.* **9**, 84–88 (2018).
- 2 I. R. Ariyaratna, F. Pawłowski, J. V. Ortiz, and E. Miliordos, *Phys. Chem. Chem. Phys.* **20**, 24186–24191 (2018).
- 3 A. M. Stacy, D. C. Johnson, and M. J. Sienko, *J. Chem. Phys.* **76**, 4248–4254 (1982).
- 4 A. M. Stacy and M. J. Sienko, *Inorg. Chem.* **21**, 2294–2297 (1982).
- 5 E. Zurek, P. P. Edwards, and R. Hoffmann, *Angew. Chem., Int. Ed.* **48**, 8198–8232 (2009).
- 6 N. M. S. Almeida and E. Miliordos, *Phys. Chem. Chem. Phys.* **21**, 7098–7104 (2019).
- 7 N. M. S. Almeida, F. Pawłowski, J. V. Ortiz, and E. Miliordos, *Phys. Chem. Chem. Phys.* **21**, 7090–7097 (2019).
- 8 I. R. Ariyaratna, N. M. S. Almeida, and E. Miliordos, *J. Phys. Chem. A* **123**, 6744–6750 (2019).
- 9 B. A. Jackson and E. Miliordos, *J. Chem. Phys.* **155**, 014303 (2021).
- 10 S. N. Khan and E. Miliordos, *J. Phys. Chem. A* **124**, 4400–4412 (2020).
- 11 Z. Jordan, S. N. Khan, B. A. Jackson, and E. Miliordos, *Electron. Struct.* **4**, 015001 (2022).
- 12 T. Yanai, D. P. Tew, and N. C. Handy, *Chem. Phys. Lett.* **393**, 51–57 (2004).
- 13 T. H. Dunning, *J. Chem. Phys.* **90**, 1007–1023 (1989).
- 14 R. A. Kendall, T. H. Dunning, and R. J. Harrison, *J. Chem. Phys.* **96**, 6796–6806 (1992).
- 15 B. P. Prascher, D. E. Woon, K. A. Peterson, T. H. Dunning, and A. K. Wilson, *Theor. Chem. Acc.* **128**, 69–82 (2011).
- 16 I. R. Ariyaratna, F. Pawłowski, J. V. Ortiz, and E. Miliordos, *J. Phys. Chem. A* **124**, 505–512 (2020).
- 17 P. Celani and H.-J. Werner, *J. Chem. Phys.* **112**, 5546–5557 (2000).
- 18 G. Ghigo, B. O. Roos, and P.-Å. Malmqvist, *Chem. Phys. Lett.* **396**, 142–149 (2004).
- 19 B. O. Roos and K. Andersson, *Chem. Phys. Lett.* **245**, 215–223 (1995).
- 20 D. E. Woon and T. H. Dunning, *J. Chem. Phys.* **100**, 2975–2988 (1994).
- 21 I. R. Ariyaratna and E. Miliordos, *J. Phys. Chem. A* **124**, 9783–9792 (2020).
- 22 A. Kramida, Y. Ralchenko, J. Reader, and NIST ASD Team, NIST Atomic Spectra Database (ver. 5.7.1), National Institute of Standards and Technology, Gaithersburg, MD, 2019, available at <https://physics.nist.gov/asd> (11 October 2020).
- 23 D. A. Dixon, D. Feller, and K. A. Peterson, *J. Phys. Chem. A* **101**, 9405–9409 (1997).
- 24 I. R. Ariyaratna and E. Miliordos, *Phys. Chem. Chem. Phys.* **21**, 15861–15870 (2019).
- 25 E. Miliordos, K. Ruedenberg, and S. S. Xantheas, *Angew. Chem., Int. Ed.* **52**, 5736–5739 (2013).
- 26 M. V. Ivanov, A. I. Krylov, and S. Zilberg, *J. Phys. Chem. Lett.* **11**, 2284–2290 (2020).
- 27 M. Díaz-Tinoco and J. V. Ortiz, *J. Phys. Chem. A* **123**, 10961–10967 (2019).
- 28 R. M. Balabin, *J. Chem. Phys.* **129**, 164101 (2008).